Comput Mech (2010) 45:141–156
DOI 10.1007/s00466-009-0429-9

ORIGINAL PAPER

Analysis of plates and shells using an edge-based smoothed finite element method

Xiangyang Cui · Gui-Rong Liu · Guang-yao Li · GuiYong Zhang · Gang Zheng

Received: 16 December 2008 / Accepted: 6 October 2009 / Published online: 23 October 2009

Abstract In this paper, an approach to the analysis of arbitrary thin to moderately thick plates and shells by the edge-based smoothed finite element method (ES-FEM) is presented. The formulation is based on the first order shear deformation theory, and Discrete Shear Gap (DSG) method is employed to mitigate the shear locking. Triangular meshes are used as they can be generated automatically for complicated geometries. The discretized system equations are obtained using the smoothed Galerkin weak form, and the numerical integration is applied based on the edge-based smoothing domains. The smoothing operation can provide a much needed softening effect to the FEM model to reduce the well-known "overly stiff" behavior caused by the fully compatible implementation of the displacement approach based on the Galerkin weakform, and hence improve significantly the solution accuracy. A number of benchmark problems have been studied and the results confirm that the present method can provide accurate results for both plate and shell using triangular mesh.

X. Cui · G. Li (✉) · G. Zheng
State Key Laboratory of Advanced Design and Manufacturing for Vehicle Body, Hunan University, 410082 Changsha, People's Republic of China
e-mail: gyli@hnu.cn

X. Cui · G.-R. Liu
Department of Mechanical Engineering, Centre for Advanced Computations in Engineering Science (ACES), National University of Singapore, 9 Engineering Drive 1, Singapore 117576, Singapore
e-mail: pwcuixy@gmail.com

G.-R. Liu · G. Zhang
Singapore-MIT Alliance (SMA), E4-04-10, 4 Engineering Drive 3, Singapore 117576, Singapore

Keywords Smoothed Galerkin weak form · Finite element · ES-FEM · Plate and shell · DSG

1 Introduction

Plates and shells are the most widely used structural components in civil, mechanical and aerospace engineering. In the past several decades, the finite element method has been used as a powerful numerical tool to simulate behaviors of plates and shells. Due to the complexity of the existing plate and shell elements, research on simpler, more efficient and inexpensive plate and shell elements receives continuously strong interest. Compared with quadrilateral element, triangular element is particularly attractive because of its simplicity, easy in automatic meshing and re-meshing in adaptive analysis. However, the development of effective triangular elements for plates and shell is not a trivial matter. The major difficulties are to overcome (1) the overly stiff behavior, and (2) the shear locking phenomenon.

Shear locking is a very well known phenomenon caused by parasitic internal energy leads to an additional, artificial stiffness. Many efficient works have been done to overcome the shear locking and various triangular elements have been proposed. Pugh et al. [1] proposed a triangular plate bending element with reduced integration. Belytschko et al. [2] used a single Gauss point integration for calculating the shear strain energy. However, the elements with reduced integration or selective integration have low accuracy and often exhibit zero energy modes. Moreover, they often can not pass the patch test for thin plates. Discrete Kirchhoff triangular (DKT) elements were developed by Stricklin et al. [3] and Dhatt [4,5], where the shear locking was eliminated by removing the shear deformation from element kinematics. Efficient results were obtained using these elements only

for thin structures since transverse shear flexibility cannot be neglected in the analysis of thick shells. Batoz et al. [6] summarized the developments of flat triangular plate bending elements with displacement degrees of freedom at the three corner nodes, and concluded that only a few elements are reliable in this class. Based on mixed interpolation of tensorial components (MITC), Bathe and co-workers developed a series of triangular elements [7,8]. MITC3 is a three-node triangular element which has a simple formulation, but some locking is present in the solution of the clamped plate problems and the hyperboloid shell problems [9]. Ayad et al. [10] proposed a MiSP (Mixed Shear Projected) approach based on the Hellinger-Reissner variational principle. The shear strains in this method were defined in terms of the edge tangential strains that were projected on the element degrees of freedom. Using assumed natural strains (ANS) model, Sze and Zhu [11] proposed a quadratic curved triangular shell element, and Kim et al. [12,13] proposed a 3-node macro triangular element for analysis of plates and shells. Chen and Cheung [14] proposed two refined triangular thin/thick plate elements (DKTM and RDTKM) based on the Timoshenko's beam theory. Based on this work, Chen [15] proposed a 15-DOF triangular discrete degenerated shell element. Bletzinger et al. [16] presented a 3-node non-isotropic triangular element DSG3 using the Discrete Shear Gap method (DSG). This element may be classified as an ANS element, but it needs not to choose an interpolation for the shear strains or to specify any sampling points. It is based on the explicit satisfaction of the kinematic equation for the shear strains at discrete points and effectively eliminates the parasitic shear strains. This element is very simple and does not need to choose an interpolation for the shear strains or to use additional sampling points.

The overly stiff behavior is observed in all fully compatible displacement-based FEM models. The primary cause of the overly stiff behavior is the fully compatible implementation of the assumed displacement field based on the standard Galerkin weakform. The overly stiff behavior is particularly severe when displacement-based triangular elements is used, which often leads to very poor accuracy in the solution. In order to reduce the stiffness of the model and widen the solution space, Liu [17] proposed a generalized smoothed Galerkin weak form (GS-Galerkin), revealed and proved a number of important properties including variational consistence, convergence, upper bound and soften effects [18]. The smoothing operation [19] has been generalized to include discontinuous functions [17], and is used for the gradient of field variables, and the smoothing operations are performed in various ways for creating models of desired properties. Using the node-based smoothing operation and the point interpolation method for shape function construction, a node-based smoothed point interpolation method (NS-PIM or LC-PIM [20]) was formulated. Liu and Zhang [21] found that NS-PIM is variationally consistent when the solution is sought from a proper H space, and can provide much better stress results. More importantly it can provide upper bound solution in energy norm. Using the FEM shape function and the element-based smoothing operations, a smoothed finite element method (SFEM) was proposed [22]. The SFEM further divides the elements into some smoothing domains, computes the integrals along the edge of the smoothing domains, and has been proven to have excellent properties. The SFEM of general n-sided polygonal elements has also been formulated, and works well for very heavily distorted mesh [23]. Liu et al. [24] gave detailed theoretical aspects including stability, bound property and convergence about SFEM. Cui et al. [25] extended the SFEM for linear and nonlinear analysis of plates and shells. Nguyen-Xuan et al. [26] extend the SFEM for plate problem coupled with MITC4 element [27]. All these models have a common foundation of the so-called G space theory [28], and fall into the category of weakened weak (W^2) formulation [18].

An edge-based smoothed finite element method (ES-FEM) [29,30] has been proposed for 2D solid mechanics problems using also the smoothed Galerkin weak form with edge-based smoothing domains. It has been found that the simple change of smoothing domains gives the ES-FEM excellent properties including good accuracy and free of spurious modes. In this work, the ES-FEM has been further extended to solve plates and shells. The present formulation is based on the first order shear deformation theory, and the shear locking is suppressed using DSG [16]. The domain is first discretized into a set of triangular elements and linear shape functions are used as same as in the standard FEM. The smoothing domains associated with the edges of the triangles are then further formed and the system stiffness matrix is obtained by integrating numerically over each smoothing domains. Compared with FEM, the smoothing operation reduces the stiffness of the discretized system, and compensates nicely the "overly stiff" behavior of the FEM model. Hence, the ES-FEM can produce better solutions than corresponding FEM model. For shell problems, an edge local coordinate system is introduced for performing strain smoothing operations. To validate the accuracy and stability of the present method, a number of numerical examples have been examined and comparisons are made with results available in literatures. The excellent results have been obtained for both plate and shell problems.

2 Formulations

2.1 Basic equations for plate and shell

The first order shear deformation theory [31] is used in this work, and thus the displacements in Cartesian coordinate system can be expressed as follows

$$\begin{aligned} u &= u_0 + z\theta_y \\ v &= v_0 - z\theta_x \\ w &= w_0 \end{aligned} \tag{1}$$

where u_0, v_0 and w_0 are the displacements of the mid-plane of the plate or shell in the x, y and z directions, θ_x and θ_y denote the rotations respect to x and y directions, respectively.

The relevant strain vector ε can be written in terms of the mid-plane deformations of Eq. (1), which gives

$$\boldsymbol{\varepsilon} = \begin{Bmatrix} \varepsilon_{xx} \\ \varepsilon_{yy} \\ \gamma_{xy} \\ \gamma_{xz} \\ \gamma_{yz} \end{Bmatrix} = \begin{Bmatrix} \boldsymbol{\varepsilon}_m \\ \mathbf{0} \end{Bmatrix} + \begin{Bmatrix} \boldsymbol{\varepsilon}_b \\ \mathbf{0} \end{Bmatrix} + \begin{Bmatrix} \mathbf{0} \\ \boldsymbol{\varepsilon}_s \end{Bmatrix} \tag{2}$$

where $\boldsymbol{\varepsilon}_m$ the membrane strain, $\boldsymbol{\varepsilon}_b$ the bending strain (curvature), and $\boldsymbol{\varepsilon}_s$ the shear strain are given by

$$\begin{aligned} \boldsymbol{\varepsilon}_m &= \begin{Bmatrix} \dfrac{\partial u_0}{\partial x} \\ \dfrac{\partial v_0}{\partial y} \\ \dfrac{\partial u_0}{\partial y} + \frac{\partial v_0}{\partial x} \end{Bmatrix}, \quad \boldsymbol{\varepsilon}_b = \begin{Bmatrix} \dfrac{\partial \theta_y}{\partial x} \\ -\dfrac{\partial \theta_x}{\partial y} \\ \dfrac{\partial \theta_y}{\partial y} - \frac{\partial \theta_x}{\partial x} \end{Bmatrix}, \\ \boldsymbol{\varepsilon}_s &= \begin{Bmatrix} \dfrac{\partial w_0}{\partial x} + \theta_y \\ \dfrac{\partial w_0}{\partial y} - \theta_y \end{Bmatrix} \end{aligned} \tag{3}$$

Applying the principle of virtual work, the weak form is stated as follows

$$\begin{aligned} &\int_\Omega \delta\boldsymbol{\varepsilon}_m^{\mathrm{T}} \mathbf{D}_m \boldsymbol{\varepsilon}_m \mathrm{d}\Omega + \int_\Omega \delta\boldsymbol{\varepsilon}_b^{\mathrm{T}} \mathbf{D}_b \boldsymbol{\varepsilon}_b \mathrm{d}\Omega + \int_\Omega \delta\boldsymbol{\varepsilon}_s^{\mathrm{T}} \mathbf{D}_s \boldsymbol{\varepsilon}_s \mathrm{d}\Omega \\ &\quad - \int_\Omega \delta\mathbf{u}^{\mathrm{T}} \tilde{\mathbf{f}} \mathrm{d}\Omega - \int_\Gamma \delta\mathbf{u}^{\mathrm{T}} \tilde{\mathbf{t}} \mathrm{d}\Gamma = 0 \end{aligned} \tag{4}$$

where the membrane stiffness constitutive coefficients ($\mathbf{D}_m$), the bending stiffness constitutive coefficients ($\mathbf{D}_b$) and the transverse shear stiffness constitutive coefficients ($\mathbf{D}_s$) are defined as

$$\mathbf{D}_m = \int_{-\frac{t}{2}}^{\frac{t}{2}} \mathbf{D}_0 \mathrm{d}z = t\mathbf{D}_0 \tag{5}$$

$$\mathbf{D}_b = \int_{-\frac{t}{2}}^{\frac{t}{2}} z^2 \mathbf{D}_0 \mathrm{d}z = \frac{t^3}{12}\mathbf{D}_0 \tag{6}$$

$$\mathbf{D}_s = \int_{-\frac{t}{2}}^{\frac{t}{2}} \chi G \begin{bmatrix} 1 & 0 \\ 0 & 1 \end{bmatrix} \mathrm{d}z = \chi t G \begin{bmatrix} 1 & 0 \\ 0 & 1 \end{bmatrix} \tag{7}$$

in which G is shear modulus, $\chi = 5/6$ is the shear correction factor, and the matrix $\mathbf{D}_0$ is the constitutive coefficients given by

$$\mathbf{D}_0 = \frac{E}{1-\nu^2} \begin{bmatrix} 1 & \nu & 0 \\ \nu & 1 & 0 \\ 0 & 0 & 1-\nu/2 \end{bmatrix} \tag{8}$$

where E is Young's modulus, and ν is Poisson ratio.

The stresses can be given as follows,

$$\boldsymbol{\sigma}_m = \{N_x,\ N_y,\ N_{xy}\}^{\mathrm{T}} = \mathbf{D}_m \boldsymbol{\varepsilon}_m \tag{9}$$

is the membrane force,

$$\boldsymbol{\sigma}_b = \{M_x,\ M_y,\ M_{xy}\}^{\mathrm{T}} = \mathbf{D}_b \boldsymbol{\varepsilon}_b \tag{10}$$

is the bending moment, and

$$\boldsymbol{\sigma}_s = \{Q_x,\ Q_y\}^{\mathrm{T}} = \mathbf{D}_s \boldsymbol{\varepsilon}_s \tag{11}$$

is the transverse shear force.

At any point in a triangular element, the generalized displacement field $\mathbf{u}$ in the element is interpolated using the nodal displacements at the nodes of the element by the linear shape functions. The same shape functions are used for both displacements and rotations

$$\mathbf{u} = \{u,\ v,\ w,\ \theta_x,\ \theta_y\}^{\mathrm{T}} = [\mathbf{N}_1\ \mathbf{N}_2\ \mathbf{N}_3] \begin{Bmatrix} \mathbf{d}_1 \\ \mathbf{d}_2 \\ \mathbf{d}_3 \end{Bmatrix} \tag{12}$$

where $\mathbf{d}_i = \{u_{0i},\ v_{0i},\ w_{0i},\ \theta_{xi},\ \theta_{yi}\}^{\mathrm{T}}$ is the generalized nodal displacement at node i, $\mathbf{N}_i(\mathbf{x})$ is a diagonal matrix of shape functions given by

$$\mathbf{N}_i = \mathrm{diag}\left\{N_i(\mathbf{x}), N_i(\mathbf{x}), N_i(\mathbf{x}), N_i(\mathbf{x}), N_i(\mathbf{x})\right\} \tag{13}$$

in which $N_i(\mathbf{x})$ is the shape function for node i. Since 3-node triangular element is used, the shape function is linear and can be given as follows [32]

$$\begin{aligned} N_i(\mathbf{x}) &= a_i + b_i x + c_i y \\ a_i &= \frac{1}{2A_e}\left(x_j y_k - x_k y_j\right), \quad b_i = \frac{1}{2A_e}\left(y_j - y_k\right), \\ c_i &= \frac{1}{2A_e}\left(x_k - x_j\right) \end{aligned} \tag{14}$$

where A_e is the area of the triangular element, the subscript i varies from 1 to 3, j and k are determined by the cyclic permutation in the order of i, j, k.

Substituting Eq. (12) into Eq. (3), the membrane strain $\boldsymbol{\varepsilon}_m$ and the bending strain $\boldsymbol{\varepsilon}_b$ can be written as

$$\boldsymbol{\varepsilon}_m = \mathbf{B}_m \mathbf{d} = [\mathbf{B}_{m1},\ \mathbf{B}_{m2},\ \mathbf{B}_{m3}] \begin{bmatrix} \mathbf{d}_1 \\ \mathbf{d}_2 \\ \mathbf{d}_3 \end{bmatrix} \tag{15}$$

$$\boldsymbol{\varepsilon}_b = \mathbf{B}_b \mathbf{d} = [\mathbf{B}_{b1},\ \mathbf{B}_{b2},\ \mathbf{B}_{b3}] \begin{bmatrix} \mathbf{d}_1 \\ \mathbf{d}_2 \\ \mathbf{d}_3 \end{bmatrix} \tag{16}$$

in which

$$\mathbf{B}_{mi} = \begin{bmatrix} N_{i,x} & 0 & 0 & 0 & 0 \\ 0 & N_{i,y} & 0 & 0 & 0 \\ N_{i,y} & N_{i,x} & 0 & 0 & 0 \end{bmatrix} \tag{17}$$

$$\mathbf{B}_{bi} = \begin{bmatrix} 0 & 0 & 0 & 0 & N_{i,x} \\ 0 & 0 & 0 & -N_{i,y} & 0 \\ 0 & 0 & 0 & -N_{i,x} & N_{i,y} \end{bmatrix} \tag{18}$$

where "( ),'' indicates differentiation, the subscript $i = 1, 2, 3$.

In order to eliminate the shear-locking, the "Discrete Shear Gap" (DSG) method [16] is used here. In each triangular element, the shear strain here can be given as:

$$\begin{aligned} \gamma_{xz} &= \sum_{i=1}^{3} N_{i,x}(\mathbf{x})\,\Delta w_{xi} + \sum_{i=1}^{3} N_{i,x}(\mathbf{x})\,\Delta w_{yi} \\ \gamma_{yz} &= \sum_{i=1}^{3} N_{i,y}(\mathbf{x})\,\Delta w_{xi} + \sum_{i=1}^{3} N_{i,y}(\mathbf{x})\,\Delta w_{yi} \end{aligned} \tag{19}$$

where Δw_{xi} and Δw_{yi} are the discrete shear gaps at the node i given by

$$\Delta w_{x1} = \Delta w_{x3} = \Delta w_{y1} = \Delta w_{y2} = 0$$

$$\begin{aligned} \Delta w_{x2} &= (w_2 - w_1) - \frac{1}{2}b\,(\theta_x 1 + \theta_x 2) \\ &\quad + \frac{1}{2}a\,(\theta_y 1 + \theta_y 2) \end{aligned} \tag{20}$$

$$\Delta w_{y3} = (w_3 - w_1) - \frac{1}{2}d\,(\theta_x 1 + \theta_x 3) + \frac{1}{2}c\,(\theta_y 1 + \theta_y 3)$$

where

$$\begin{aligned} a &= x_2 - x_1, \quad b = y_2 - y_1 \\ c &= x_3 - x_1, \quad d = y_3 - y_1 \end{aligned} \tag{21}$$

From Eqs. (19), (20) and (21), the shear strain $\boldsymbol{\varepsilon}_s$ in each element can be written as

$$\boldsymbol{\varepsilon}_s = \begin{Bmatrix} \gamma_{xz} \\ \gamma_{yz} \end{Bmatrix} = \mathbf{B}_s\mathbf{d} = [\mathbf{B}_{s1},\ \mathbf{B}_{s2},\ \mathbf{B}_{s3}] \begin{Bmatrix} \mathbf{d}_1 \\ \mathbf{d}_2 \\ \mathbf{d}_3 \end{Bmatrix} \tag{22}$$

in which

$$\mathbf{B}_{s1} = \frac{1}{2A_e}\begin{bmatrix} 0 & 0 & b-d & 0 & A_e & 0 \\ 0 & 0 & c-a & -A_e & 0 & 0 \end{bmatrix} \tag{23a}$$

$$\mathbf{B}_{s2} = \frac{1}{2A_e}\begin{bmatrix} 0 & 0 & d & -\frac{bd}{2} & \frac{ad}{2} & 0 \\ 0 & 0 & -c & \frac{bc}{2} & -\frac{ac}{2} & 0 \end{bmatrix} \tag{23b}$$

$$\mathbf{B}_{s3} = \frac{1}{2A_e}\begin{bmatrix} 0 & 0 & -b & \frac{bd}{2} & -\frac{bc}{2} & 0 \\ 0 & 0 & a & -\frac{ad}{2} & \frac{ac}{2} & 0 \end{bmatrix} \tag{23c}$$

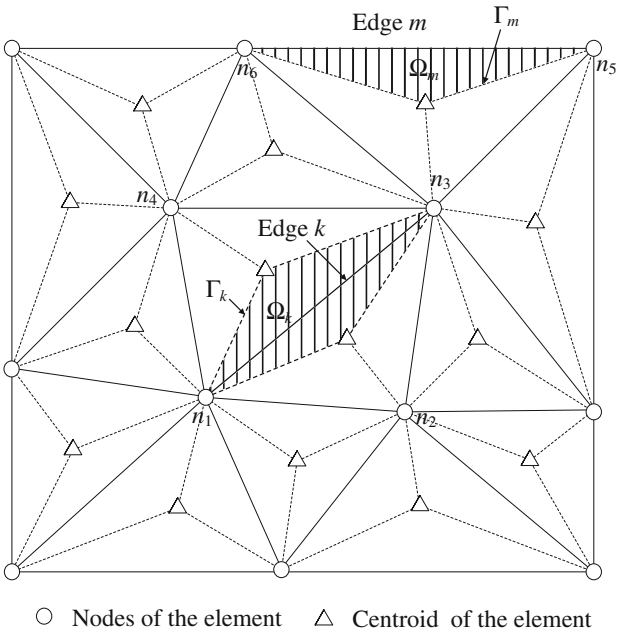

Fig. 1 A problem domain is divided into N_{eiem} triangular elements with a total of N_{edge} edges. Interior *element* edge k is sandwiched in the smoothing domain Ω_k bounded by Γ_k. Smoothing domain Ω_m for the boundary edge m is a triangle. There are N_k nodes that influence the kth smoothing domain Ω_k. For domains associated with boundary edges $N_k = 3$; for example, nodes n_3, n_5 and n_6 influence Ω_m. For domains associated with interior edges $N_k = 4$; for example, nodes n_1, n_2, n_3 and n_4 influence Ω_k

2.2 Edge-based strain smoothing technique for plate

In this section, the edge-based strain smoothing technique will be introduced. In present ES-FEM, the problem domain Ω is divided into N_{elem} triangular elements with a total of N_{edge} edges. In order to perform the smoothing operation, a smoothing domain for each edge is formed by sequentially connecting two end points of the edge and centroids of its surrounding triangles, such that $\Omega = \Omega_1 \cup \Omega_2 \cup \ldots \cup \Omega_{N_{\text{edge}}}$ and $\Omega_i \cap \Omega_j = \emptyset$, $(i \neq j, i = 1, \ldots, N_{\text{edge}},\ j = 1, \ldots, N_{\text{edge}})$, as shown in Fig. 1. In the ES-FEM, the displacement interpolation is element based, but the integration is based on the smoothing domains. As shown in Fig. 2, for interior edges, the integration domain Ω_k of edge k is formed by assembling two sub-domains Ω_{k1} and Ω_{k2} of two neighboring elements. The sub-domain Ω_{k1} and the sub-domain Ω_{k2} are from element $e1$ and element $e2$, respectively.

Introducing the strain smoothing operation [17], the smoothed strain in the smoothing domain Ω_k are given by

$$\begin{aligned} \bar{\boldsymbol{\varepsilon}}_m^{(k)} &= \frac{1}{A_k}\int_{\Omega_k} \boldsymbol{\varepsilon}_m^{(k)} \mathrm{d}\Omega \\ &= \frac{1}{A_k}\left(\int_{\Omega_{k1}} \boldsymbol{\varepsilon}_m^{(k1)}(\mathbf{x})\,\mathrm{d}\Omega + \int_{\Omega_{k2}} \boldsymbol{\varepsilon}_m^{(k2)}(\boldsymbol{x})\,\mathrm{d}\Omega\right) \end{aligned} \tag{24a}$$

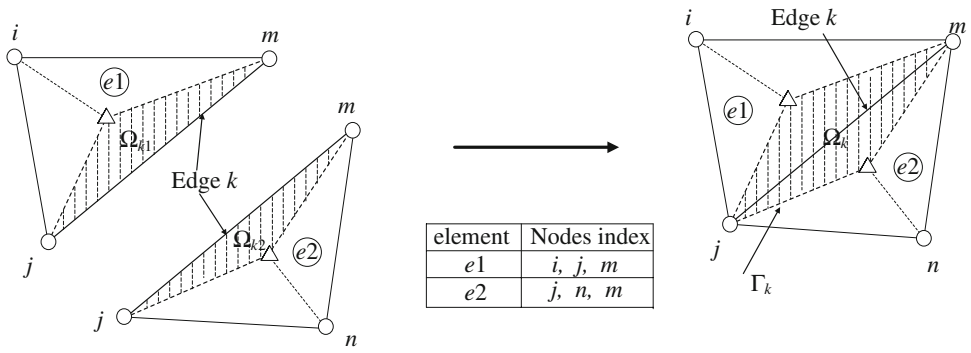

Fig. 2 The integration is performed over each of the edge-based smoothing domains. Domain Ω_k of edge k is formed by assembling two sub-domains Ω_{k1} and Ω_{k2} of two neighboring elements. The sub-domain Ω_{k1} is from element $e1$ and the sub-domain Ω_{k2} is from element $e2$

$$\bar{\boldsymbol{\varepsilon}}_b^{(k)} = \frac{1}{A_k}\int_{\Omega_k} \boldsymbol{\varepsilon}_b^{(k)} \mathrm{d}\Omega = \frac{1}{A_k}\left(\int_{\Omega_{k1}} \boldsymbol{\varepsilon}_b^{(k1)}(\mathbf{x})\,\mathrm{d}\Omega + \int_{\Omega_{k2}} \boldsymbol{\varepsilon}_b^{(k2)}(\mathbf{x})\,\mathrm{d}\Omega\right) \tag{24b}$$

$$\bar{\boldsymbol{\varepsilon}}_s^{(k)} = \frac{1}{A_k}\int_{\Omega_k} \boldsymbol{\varepsilon}_s^{(k)} \mathrm{d}\Omega = \frac{1}{A_k}\left(\int_{\Omega_{k1}} \boldsymbol{\varepsilon}_s^{(k1)}(\mathbf{x})\,\mathrm{d}\Omega + \int_{\Omega_{k2}} \boldsymbol{\varepsilon}_s^{(k2)}(\mathbf{x})\,\mathrm{d}\Omega\right) \tag{24c}$$

where A_k is the area of the smoothing domain Ω_k, $\boldsymbol{\varepsilon}_m^{(k1)}(\mathbf{x})$, $\boldsymbol{\varepsilon}_b^{(k1)}(\mathbf{x})$ and $\boldsymbol{\varepsilon}_s^{(k1)}(\mathbf{x})$ are the compatible strains calculated in element $e1$, $\boldsymbol{\varepsilon}_m^{(k2)}(\mathbf{x})$, $\boldsymbol{\varepsilon}_b^{(k2)}(\mathbf{x})$ and $\boldsymbol{\varepsilon}_s^{(k2)}(\mathbf{x})$ are the compatible strain calculated in element $e2$.

Since linear shape functions are used in the present method, the compatible strain is a constant in each smoothing sub-domain. Therefore, Eq. (24) can be rewritten as

$$\bar{\boldsymbol{\varepsilon}}_m^{(k)} = \frac{1}{A_k}\left(A_{k1}\boldsymbol{\varepsilon}_m^{(k1)} + A_{k2}\boldsymbol{\varepsilon}_m^{(k2)}\right) \tag{25a}$$

$$\bar{\boldsymbol{\varepsilon}}_b^{(k)} = \frac{1}{A_k}\left(A_{k1}\boldsymbol{\varepsilon}_b^{(k1)} + A_{k2}\boldsymbol{\varepsilon}_b^{(k2)}\right) \tag{25b}$$

$$\bar{\boldsymbol{\varepsilon}}_s^{(k)} = \frac{1}{A_k}\left(A_{k1}\boldsymbol{\varepsilon}_s^{(k1)} + A_{k2}\boldsymbol{\varepsilon}_s^{(k2)}\right) \tag{25c}$$

where A_{k1} and A_{k2} are areas of the smoothing sub-domains Ω_{k1} and Ω_{k2}, respectively.

Substituting Eqs. (15), (16) and (22) into Eq. (25), the smoothed strains can be given by

$$\bar{\boldsymbol{\varepsilon}}_m^{(k)} = \frac{A_{k1}}{A_k}\mathbf{B}_m^{(k1)}\mathbf{d}^{(k1)} + \frac{A_{k2}}{A_k}\mathbf{B}_m^{(k2)}\mathbf{d}^{(k2)} = \bar{\mathbf{B}}_m^{(k)}\mathbf{d}^{(k)} \tag{26a}$$

$$\bar{\boldsymbol{\varepsilon}}_b^{(k)} = \frac{A_{k1}}{A_k}\mathbf{B}_b^{(k1)}\mathbf{d}^{(k1)} + \frac{A_{k2}}{A_k}\mathbf{B}_b^{(k2)}\mathbf{d}^{(k2)} = \bar{\mathbf{B}}_b^{(k)}\mathbf{d}^{(k)} \tag{26b}$$

$$\bar{\boldsymbol{\varepsilon}}_s^{(k)} = \frac{A_{k1}}{A_k}\mathbf{B}_s^{(k1)}\mathbf{d}^{(k1)} + \frac{A_{k2}}{A_k}\mathbf{B}_s^{(k2)}\mathbf{d}^{(k2)} = \bar{\mathbf{B}}_s^{(k)}\mathbf{d}^{(k)} \tag{26c}$$

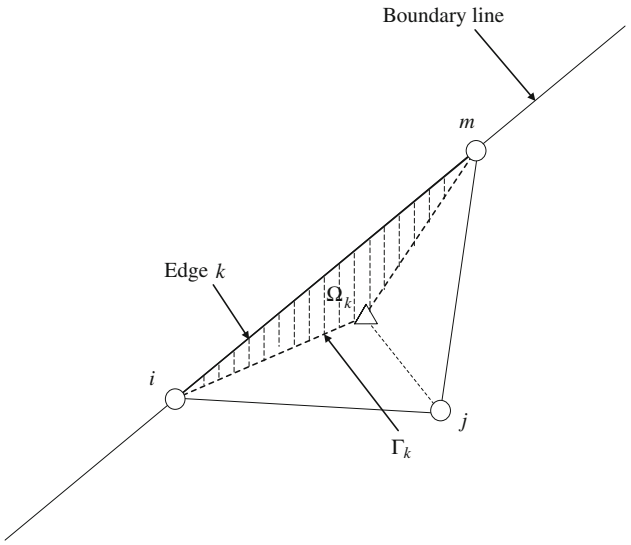

Fig. 3 The integration domain Ω_k of edge k is only a single sub-domain

where $\mathbf{d}^{(k1)}$ and $\mathbf{d}^{(k2)}$ are the nodal displacements vector of the element $e1$ and the element $e2$, respectively, $\mathbf{d}^{(k)}$ are the displacements vector of the nodes associated with edge k, $\mathbf{B}_m^{(k1)}$, $\mathbf{B}_b^{(k1)}$ and $\mathbf{B}_s^{(k1)}$ are the compatible strain matrices of the smoothing sub-domain Ω_{k1} and $\mathbf{B}_m^{(k2)}$, $\mathbf{B}_b^{(k2)}$ and $\mathbf{B}_s^{(k2)}$ are the compatible strain matrices of the smoothing sub-domain Ω_{k2}, respectively. Note that the sign '+' denotes assembly but not sum here.

For boundary edges as shown in Fig. 3, the smoothing domain Ω_k of edge k is a single sub-domain, and strains in Eq. (26) are obtained by the single subdomain. In this case, the strain and strain matrix have the same form as those in FEM.

2.3 Edge-based strain smoothing technique for shell

For shell problems, local coordinate system is defined in each element, and the compatible strains are computed in this local coordinate system. In order to perform the strain smoothing over the same local coordinate system for two sub-domains

from two different elements sharing an inner edge, coordinate system $(\bar{x}, \bar{y}, \bar{z})$ associated with an edge is defined in this study. Let $\bar{x}$ be coinciding with the edge k, $\bar{z}$ be the average normal direction of the two elements sharing edge k, and $\bar{y}$ direction is then defined as the cross product of the unit vectors in the $\bar{z}$ and $\bar{x}$ directions. From simple transformation rules for each triangular element, the strain in the edge coordinate system can be written as

$$\begin{aligned}\bar{\boldsymbol{\varepsilon}}_m &= \mathbf{R}_{m1}\mathbf{R}_{m2}\hat{\boldsymbol{\varepsilon}}_m \\ \bar{\boldsymbol{\varepsilon}}_b &= \mathbf{R}_{b1}\mathbf{R}_{b2}\hat{\boldsymbol{\varepsilon}}_b \\ \bar{\boldsymbol{\varepsilon}}_s &= \mathbf{R}_{s1}\mathbf{R}_{s2}\hat{\boldsymbol{\varepsilon}}_s\end{aligned} \tag{27}$$

in which $\hat{\boldsymbol{\varepsilon}}_m$, $\hat{\boldsymbol{\varepsilon}}_b$ and $\hat{\boldsymbol{\varepsilon}}_s$ are strains in element local coordinate system, and

$$\mathbf{R}_{m1} = \mathbf{R}_{b1} = \begin{bmatrix} c_{\bar{x}\hat{x}}^2 & c_{\bar{x}\hat{y}}^2 & c_{\bar{x}\hat{z}}^2 & c_{\bar{x}\hat{x}}c_{\bar{x}\hat{y}} & c_{\bar{x}\hat{y}}c_{\bar{x}\hat{z}} & c_{\bar{x}\hat{x}}c_{\bar{x}\hat{z}} \\ c_{\bar{y}\hat{x}}^2 & c_{\bar{y}\hat{y}}^2 & c_{\bar{y}\hat{z}}^2 & c_{\bar{y}\hat{x}}c_{\bar{y}\hat{y}} & c_{\bar{y}\hat{y}}c_{\bar{y}\hat{z}} & c_{\bar{y}\hat{x}}c_{\bar{y}\hat{z}} \\ 2c_{\bar{x}\hat{x}}c_{\bar{y}\hat{x}} & 2c_{\bar{x}\hat{y}}c_{\bar{y}\hat{y}} & 2c_{\bar{x}\hat{z}}c_{\bar{y}\hat{z}} & c_{\bar{x}\hat{x}}c_{\bar{y}\hat{y}} + c_{\bar{y}\hat{x}}c_{\bar{x}\hat{y}} & c_{\bar{x}\hat{z}}c_{\bar{y}\hat{y}} + c_{\bar{y}\hat{z}}c_{\bar{x}\hat{y}} & c_{\bar{x}\hat{x}}c_{\bar{y}\hat{z}} + c_{\bar{y}\hat{x}}c_{\bar{x}\hat{z}} \end{bmatrix} \tag{28}$$

$$\mathbf{R}_{s1} = \begin{bmatrix} 2c_{\bar{x}\hat{x}}c_{\bar{z}\hat{x}} & 2c_{\bar{x}\hat{y}}c_{\bar{z}\hat{y}} & 2c_{\bar{x}\hat{z}}c_{\bar{z}\hat{z}} & c_{\bar{x}\hat{x}}c_{\bar{z}\hat{y}} + c_{\bar{z}\hat{x}}c_{\bar{x}\hat{y}} & c_{\bar{x}\hat{z}}c_{\bar{z}\hat{y}} + c_{\bar{z}\hat{z}}c_{\bar{x}\hat{y}} & c_{\bar{x}\hat{x}}c_{\bar{z}\hat{z}} + c_{\bar{z}\hat{x}}c_{\bar{x}\hat{z}} \\ 2c_{\bar{y}\hat{x}}c_{\bar{z}\hat{x}} & 2c_{\bar{y}\hat{y}}c_{\bar{z}\hat{y}} & 2c_{\bar{y}\hat{z}}c_{\bar{z}\hat{z}} & c_{\bar{y}\hat{x}}c_{\bar{z}\hat{y}} + c_{\bar{z}\hat{x}}c_{\bar{y}\hat{y}} & c_{\bar{y}\hat{z}}c_{\bar{z}\hat{y}} + c_{\bar{z}\hat{z}}c_{\bar{y}\hat{y}} & c_{\bar{y}\hat{x}}c_{\bar{z}\hat{z}} + c_{\bar{z}\hat{x}}c_{\bar{y}\hat{z}} \end{bmatrix} \tag{29}$$

$$\mathbf{R}_{m2} = \mathbf{R}_{b2} = \begin{bmatrix} c_{\hat{x}\hat{x}}^2 & c_{\hat{y}\hat{x}}^2 & c_{\hat{x}\hat{x}}c_{\hat{y}\hat{x}} \\ c_{\hat{x}\hat{y}}^2 & c_{\hat{y}\hat{y}}^2 & c_{\hat{x}\hat{y}}c_{\hat{y}\hat{y}} \\ c_{\hat{x}\hat{z}}^2 & c_{\hat{y}\hat{z}}^2 & c_{\hat{x}\hat{z}}c_{\hat{y}\hat{z}} \\ 2c_{\hat{x}\hat{x}}c_{\hat{x}\hat{y}} & 2c_{\hat{y}\hat{x}}c_{\hat{y}\hat{y}} & c_{\hat{x}\hat{x}}c_{\hat{y}\hat{y}} + c_{\hat{x}\hat{y}}c_{\hat{y}\hat{x}} \\ 2c_{\hat{x}\hat{y}}c_{\hat{x}\hat{z}} & 2c_{\hat{y}\hat{y}}c_{y'z} & c_{\hat{x}\hat{y}}c_{\hat{y}\hat{z}} + c_{\hat{x}\hat{z}}c_{\hat{y}\hat{y}} \\ 2c_{\hat{x}\hat{x}}c_{\hat{x}\hat{z}} & 2c_{\hat{y}\hat{x}}c_{y'z} & c_{\hat{x}\hat{x}}c_{\hat{y}\hat{z}} + c_{\hat{x}\hat{z}}c_{\hat{y}\hat{x}} \end{bmatrix} \tag{30}$$

$$\mathbf{R}_{s2} = \begin{bmatrix} c_{\hat{x}\hat{x}}c_{\hat{z}\hat{x}} & c_{\hat{y}\hat{x}}c_{\hat{z}\hat{x}} \\ c_{\hat{x}\hat{y}}c_{\hat{z}\hat{y}} & c_{\hat{y}\hat{y}}c_{\hat{z}\hat{y}} \\ c_{\hat{x}\hat{z}}c_{\hat{z}\hat{z}} & c_{\hat{y}\hat{z}}c_{\hat{z}\hat{z}} \\ c_{\hat{x}\hat{x}}c_{\hat{z}\hat{y}} + c_{\hat{x}\hat{y}}c_{\hat{z}\hat{x}} & c_{\hat{y}\hat{x}}c_{\hat{z}\hat{y}} + c_{\hat{y}\hat{y}}c_{\hat{z}\hat{x}} \\ c_{\hat{x}\hat{z}}c_{\hat{z}\hat{y}} + c_{\hat{x}\hat{y}}c_{\hat{z}\hat{z}} & c_{\hat{y}\hat{z}}c_{\hat{z}\hat{y}} + c_{\hat{y}\hat{y}}c_{\hat{z}\hat{z}} \\ c_{\hat{x}\hat{x}}c_{\hat{z}\hat{z}} + c_{\hat{x}\hat{z}}c_{\hat{z}\hat{x}} & c_{\hat{y}\hat{x}}c_{\hat{z}\hat{z}} + c_{\hat{y}\hat{z}}c_{\hat{z}\hat{x}} \end{bmatrix} \tag{31}$$

where as usual $c_{\bar{x}x}$ is the cosine of the angle between the $\bar{x}$ and x axes, etc.

Using Eqs. (15), (16) and (22), the strains in the edge system can be obtained using those in element local coordinate system

$$\begin{aligned}\bar{\boldsymbol{\varepsilon}}_m &= \mathbf{R}_{m1}\mathbf{R}_{m2}\hat{\mathbf{B}}_m\hat{\mathbf{d}} \\ \bar{\boldsymbol{\varepsilon}}_b &= \mathbf{R}_{b1}\mathbf{R}_{b2}\hat{\mathbf{B}}_b\hat{\mathbf{d}} \\ \bar{\boldsymbol{\varepsilon}}_s &= \mathbf{R}_{s1}\mathbf{R}_{s2}\hat{\mathbf{B}}_s\hat{\mathbf{d}}\end{aligned} \tag{32}$$

where $\hat{\mathbf{B}}_m$, $\hat{\mathbf{B}}_b$ and $\hat{\mathbf{B}}_s$ are strain matrices in element local coordinate system, and

$$\hat{\mathbf{d}}_i = \hat{\mathbf{T}} d_i \tag{33}$$

where $\hat{\mathbf{d}}_i$ and $\mathbf{d}_i$ are the nodal displacement vectors at node i expressed in local and global coordinates, respectively, and transformation matrix $\hat{\mathbf{T}}$ can be written as

$$\hat{\mathbf{T}} = \begin{bmatrix} \mathbf{T}_{3\times3} & \mathbf{0}_{3\times3} \\ \mathbf{0}_{2\times3} & \mathbf{T}_{2\times3} \end{bmatrix} \tag{34}$$

in which

$$T_{ij} = c_{\hat{i}\hat{j}} \tag{35}$$

As shown in Fig. 4, the smoothing domain Ω_k corresponding to an inner edge k consists of two sub-domains. The strain in the edge coordinate system of each sub-domain Ω_{kI} can be noted as $\bar{\boldsymbol{\varepsilon}}_m^{(kI)}$, $\bar{\boldsymbol{\varepsilon}}_b^{(kI)}$ and $\bar{\boldsymbol{\varepsilon}}_s^{(kI)}$ for the Ith triangular element. As the strain is constant field in the linear triangular element, the strain in smoothing domain can be easily obtained by

$$\bar{\boldsymbol{\varepsilon}}_m^{(k)} = \frac{1}{A_k}\sum_I A_{kI}\bar{\boldsymbol{\varepsilon}}_m^{(kI)} \tag{36a}$$

$$\bar{\boldsymbol{\varepsilon}}_b^{(k)} = \frac{1}{A_k}\sum_I A_{kI}\bar{\boldsymbol{\varepsilon}}_b^{(kI)} \tag{36b}$$

$$\bar{\boldsymbol{\varepsilon}}_b^{(k)} = \frac{1}{A_k}\sum_I A_{kI}\bar{\boldsymbol{\varepsilon}}_b^{(kI)} \tag{36c}$$

where A_k is the area of the smoothing domain Ω_k, A_{kI} is the area of the sub-domain Ω_{kI}.

Using Eqs. (32), (33) and (36), the relationship between strains and global nodal displacement vectors can be given as

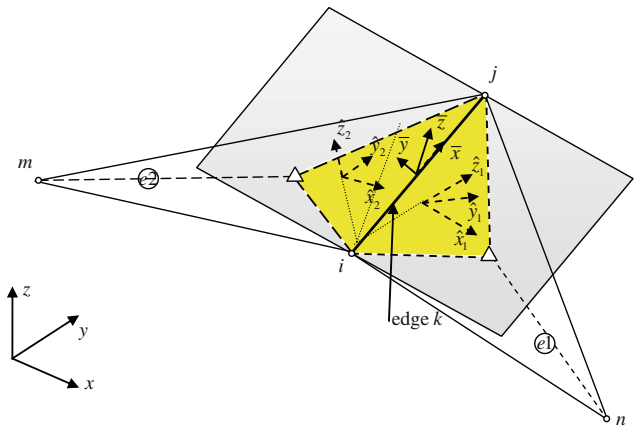

Fig. 4 Shell element for edge-based smoothing, integration domain and coordinate systems

$$\bar{\boldsymbol{\varepsilon}}_m^{(k)} = \bar{\mathbf{B}}_m^{(k)}\mathbf{d}^{(k)} \tag{37a}$$

$$\bar{\boldsymbol{\varepsilon}}_b^{(k)} = \bar{\mathbf{B}}_b^{(k)}\mathbf{d}^{(k)} \tag{37b}$$

$$\bar{\varepsilon}_s^{(k)} = \bar{\mathbf{B}}_s^{(k)}\mathbf{d}^{(k)} \tag{37c}$$

in which

$$\bar{\mathbf{B}}_m^{(k)} = \frac{1}{A_k}\sum_I A_{kI}\mathbf{R}_{m1}^{(k)}\mathbf{R}_{m2}^{(kI)}\hat{\mathbf{B}}_m^{(kI)}\hat{\mathbf{T}}^{(I)} \tag{38a}$$

$$\bar{\mathbf{B}}_b^{(k)} = \frac{1}{A_k}\sum_I A_{kI}\mathbf{R}_{b1}^{(k)}\mathbf{R}_{b2}^{(kI)}\hat{\mathbf{B}}_b^{(kI)}\hat{\mathbf{T}}^{(I)} \tag{38b}$$

$$\bar{\mathbf{B}}_s^{(k)} = \frac{1}{A_k}\sum_I A_{kI}\mathbf{R}_{s1}^{(k)}\mathbf{R}_{s2}^{(kI)}\hat{\mathbf{B}}_s^{(kI)}\hat{\mathbf{T}}^{(I)} \tag{38c}$$

where the summation in Eq. (38) means an assembly process, $\mathbf{R}_{m1}^{(k)}$, $\mathbf{R}_{b1}^{(k)}$ and $\mathbf{R}_{s1}^{(k)}$ are the transformation matrices for the kth edge given by Eqs. (28) and (29), $\mathbf{R}_{m2}^{(kI)}$, $\mathbf{R}_{b2}^{(kI)}$, $\mathbf{R}_{s2}^{(kI)}$ and $\mathbf{T}^{(kI)}$ are the transformation matrices for the Ith element sharing the edge k and they are given by Eqs. (30), (31) and (34). It must be pointed out that the global nodal displacements vector $\mathbf{d}^{(k)}$ contains all of nodes of the two elements sharing the edge k.

2.4 Smoothed Galerkin formulation

We now seek for a weak form solution of generalized displacement field $\mathbf{u}$ that satisfies the following smoothed Galerkin weak form

$$\int_\Omega \delta\bar{\boldsymbol{\varepsilon}}_m^{\mathrm{T}}\mathbf{D}_m\bar{\boldsymbol{\varepsilon}}_m \mathrm{d}\Omega + \int_\Omega \delta\bar{\boldsymbol{\varepsilon}}_b^{\mathrm{T}}\mathbf{D}_b\bar{\boldsymbol{\varepsilon}}_b \mathrm{d}\Omega + \int_\Omega \delta\bar{\boldsymbol{\varepsilon}}_s^{\mathrm{T}}\mathbf{D}_s\bar{\boldsymbol{\varepsilon}}_s \mathrm{d}\Omega - \int_\Omega \delta\mathbf{u}^{\mathrm{T}}\tilde{\mathbf{f}}\mathrm{d}\Omega - \int_\Gamma \delta\mathbf{u}^{\mathrm{T}}\tilde{\mathbf{t}}\mathrm{d}\Gamma = 0 \tag{39}$$

where $\tilde{\mathbf{f}}$ is the external load applied over the problem domain Ω, and $\tilde{\mathbf{t}}$ is the traction applied on the natural boundary Γ.

Substituting Eq. (12) and Eq. (26) (for plate) or Eq. (37) (for shell) into Eq. (39), a set of discretized algebraic system equations can be obtained in the following matrix form

$$\bar{\mathbf{K}}\mathbf{d} - \mathbf{f} = 0 \tag{40}$$

where $\mathbf{d}$ is the vector of global nodal displacement at all of the nodes, and $\mathbf{f}$ is the force vector defined as

$$\mathbf{f} = \int_\Omega \mathbf{N}(\mathbf{x})\,\tilde{\mathbf{f}}\mathrm{d}\Omega + \int_\Gamma \mathbf{N}(\mathbf{x})\,\tilde{\mathbf{t}}\mathrm{d}\Gamma \tag{41}$$

In Eq. (40), $\bar{\mathbf{K}}$ is the (global) smoothed stiffness matrix assembled in the form of

$$\bar{\mathbf{K}}_{ij} = \sum_{k=1}^{N_{\mathrm{edge}}} \bar{\mathbf{K}}_{ij}^{(k)} \tag{42}$$

The summation in Eq. (42) means an assembly process same as the practice in the FEM, N_{edge} is the number of the edges of the whole problem domain Ω, and $\bar{\mathbf{K}}_{ij}^{(k)}$ is the stiffness matrix associated with edge k given as follows

$$\bar{\mathbf{K}}_{ij}^{(k)} = \bar{\mathbf{K}}_{mij}^{(k)} + \bar{\mathbf{K}}_{bij}^{(k)} + \bar{\mathbf{K}}_{sij}^{(k)} \tag{43}$$

where

$$\begin{aligned}
\bar{\mathbf{K}}_{mij}^{(k)} &= \int_{\Omega_k} \left(\bar{\mathbf{B}}_m^{(k)}\right)_i^{\mathrm{T}} \mathbf{D}_m \left(\bar{\mathbf{B}}_m^{(k)}\right)_j \mathrm{d}\Omega \\
&= \left(\bar{\mathbf{B}}_m^{(k)}\right)_i^{\mathrm{T}} \mathbf{D}_m \left(\bar{\mathbf{B}}_m^{(k)}\right)_j A_k \\
\bar{\mathbf{K}}_{bij}^{(k)} &= \int_{\Omega_k} \left(\bar{\mathbf{B}}_b^{(k)}\right)_i^{\mathrm{T}} \mathbf{D}_b \left(\bar{\mathbf{B}}_b^{(k)}\right)_j \mathrm{d}\Omega \\
&= \left(\bar{\mathbf{B}}_b^{(k)}\right)_i^{\mathrm{T}} \mathbf{D}_b \left(\bar{\mathbf{B}}_b^{(k)}\right)_j A_k \\
\bar{\mathbf{K}}_{sij}^{(k)} &= \int_{\Omega_k} \left(\bar{\mathbf{B}}_s^{(k)}\right)_i^{\mathrm{T}} \mathbf{D}_s \left(\bar{\mathbf{B}}_s^{(k)}\right)_j \mathrm{d}\Omega \\
&= \left(\bar{\mathbf{B}}_s^{(k)}\right)_i^{\mathrm{T}} \mathbf{D}_s \left(\bar{\mathbf{B}}_s^{(k)}\right)_j A_k
\end{aligned} \tag{44}$$

3 Numerical examples

3.1 Patch test

The first numerical example is the standard patch test; the mesh of a square patch of the plate with thickness $t = 0.001$ is depicted in Fig. 5. The plate is subjected to the prescribed

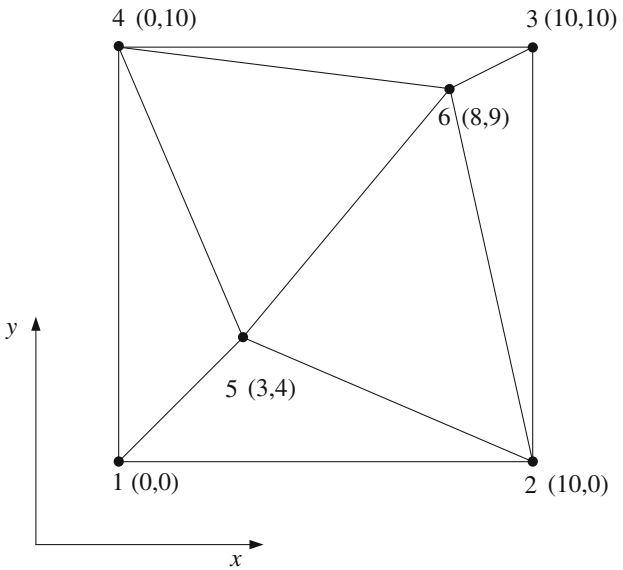

Fig. 5 Mesh for the standard patch test

displacement and rotations on boundary of the patch (at nodes 1 to 4) are computed using

$$\begin{aligned} w &= 10^{-3}(1+x+y+x^2+xy+y^2) \\ \theta_x &= -\frac{\partial w}{\partial x} = -10^{-3}(1+y+2x) \\ \theta_y &= -\frac{\partial w}{\partial y} = -10^{-3}(1+x+2y) \end{aligned} \tag{45}$$

The material properties of patch are $E = 1.0 \times 10^6$ and $\nu = 0.25$. To satisfy the patch test, the deflection and rotations at any interior nodes computed by numerical method should be exactly the analytic ones given in Eq. (45). To examine the numerical error precisely, an error norm is defined as

$$e_u = \sqrt{\sum_{i=1}^{6} \left(\frac{\left(\mathbf{u}^i_{\text{num}} - \mathbf{u}^i_{\text{exact}}\right)^{\mathrm{T}} \left(\mathbf{u}^i_{num} - \mathbf{u}^i_{\text{exact}}\right)}{\left(\mathbf{u}^i_{\text{exact}}\right)^{\mathrm{T}} \left(\mathbf{u}^i_{\text{exact}}\right)} \right)} \tag{46}$$

where $\mathbf{u}_{\text{num}}$ is the displacement vector computed by the present ES-FEM, and $\mathbf{u}_{\text{exact}}$ is the displacement vector computed from Eq. (45). Our numerical computation has found the error norm being $e_u = 4.474065656539186 \times 10^{-15}$ that is of the order of the machine accuracy. This shows a successful pass of the patch test for present method.

3.2 Square plates

A square plate of length $L = 10$ subjected to different boundary conditions is considered in this subsection. The material properties are taken as Young's modulus $E = 3.0 \times 10^7$, and Poisson ratio $\nu = 0.3$. Owing to the symmetry conditions, only a quarter of the plate is modeled. Figure 6 shows the meshes of different density used for the square plate. The results of center deflections are normalized with the formulation given by Zienkiewicz and Taylor [33]. For the plate subjected to uniform load, the deflection is normalized as $\hat{w} = w_c D/qL^4$, where q is the uniform load. For the plate subjected to concentrated central load, the deflection is normalized as $\hat{w} = w_c D/PL^2$, in which P is the concentrated central load. Both thin plate ($L/t = 100$) and thick plate ($L/t = 5$) with different boundary conditions are investigated in this subsection.

For the purpose of testing the element performance, the numerical results obtained from the present ES-FEM are compared with several existing triangular plate elements,

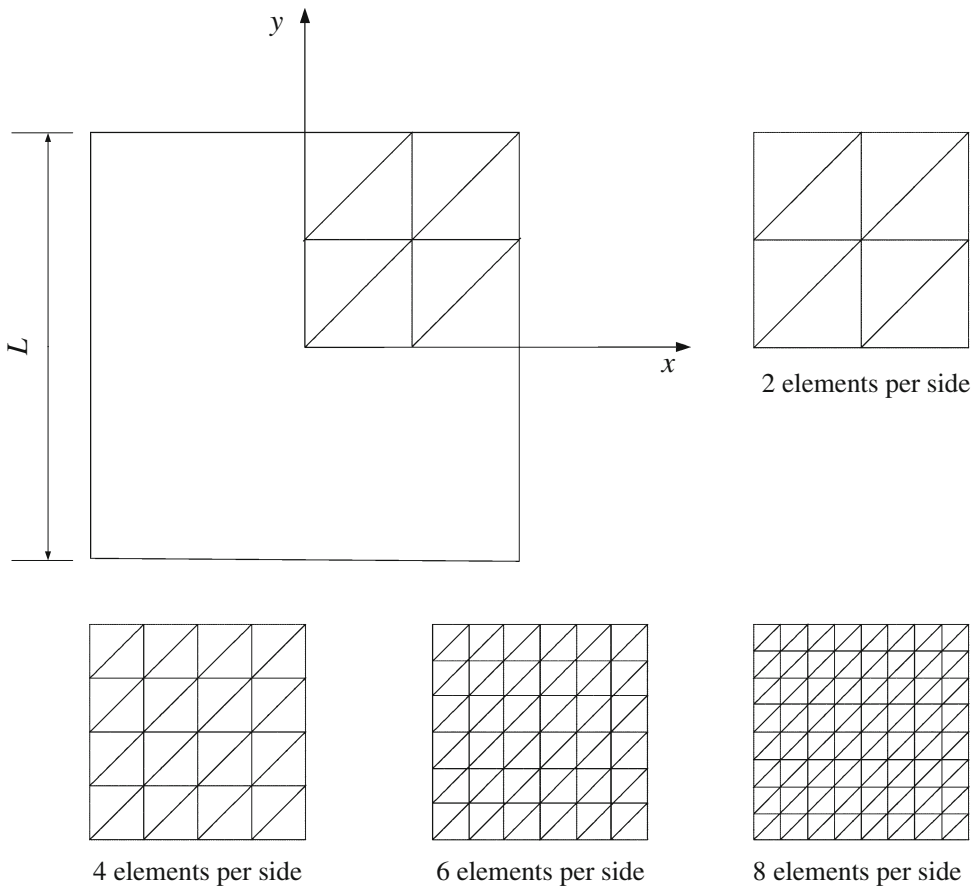

Fig. 6 Square plate mesh

Table 1 Numerical results of normalized central deflection for a simply supported square plate subjected uniform load ($L/t = 100$)

Mesh	DKT	RDKTM	DSG	Present
2×2	0.004056	0.004058	0.003705	0.004078
4×4	0.004065	0.004069	0.003975	0.004068
6×6	0.004064	0.004066	0.004024	0.004066
8×8	0.004064	0.004065	0.004042	0.004065
Analytic solution	0.004064			

Table 2 Numerical results of normalized central deflection for a simply supported square plate subjected uniform load ($L/t = 5$)

Mesh	DKT	RDKTM	DSG	Present
2×2	0.004056	0.004902	0.004499	0.00496
4×4	0.004065	0.004904	0.004804	0.00492
6×6	0.004064	0.004906	0.00486	0.004912
8×8	0.004064	0.004906	0.004879	0.004909
Analytic solution	0.004907			

Table 3 Numerical results of normalized central deflection for a clamped square plate subjected uniform load ($L/t = 100$)

Mesh	DKT	RDKTM	DSG	Present
2×2	0.001547	0.00155	0.00107	0.00135
4×4	0.001347	0.00135	0.001213	0.001299
6×6	0.001303	0.001305	0.001243	0.001285
8×8	0.001287	0.001289	0.001254	0.001279
Analytic solution	0.001265			

Table 4 Numerical results of normalized central deflection for a clamped square plate subjected uniform load. ($L/t = 5$)

Mesh	DKT	RDKTM	DSG	Present
2×2	0.001547	0.002423	0.002226	0.001862
4×4	0.001347	0.002243	0.002205	0.002093
6×6	0.001303	0.002205	0.00219	0.002136
8×8	0.001287	0.002191	0.002183	0.002152
Analytic solution	0.00217			

Table 5 Numerical results of normalized central deflection for a square plate subjected concentrated central load with different constraints ($L/t = 100$)

Mesh	Simply supported		Clamped	
	DSG	Present	DSG	Present
2×2	0.010624	0.011986	0.004252	0.005393
4×4	0.011285	0.011750	0.005205	0.005658
6×6	0.011445	0.011685	0.005416	0.005657
8×8	0.011507	0.011656	0.005496	0.005647
Analytic solution	0.011601		0.005612	

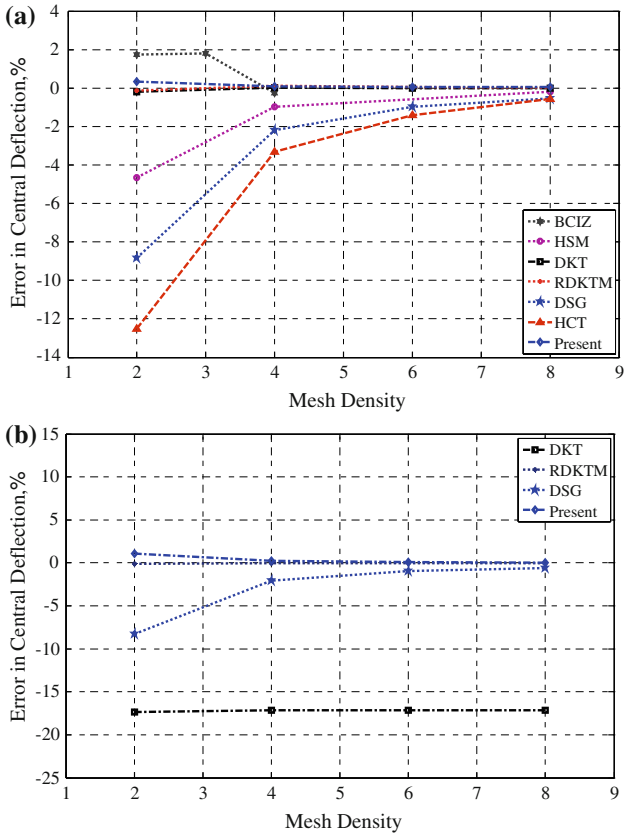

Fig. 7 Relative error of the deflection at centre for a simply supported square plate with uniform load for different element types. **a** Thin plate ($L/t = 100$). **b** Thick plate ($L/t = 5$)

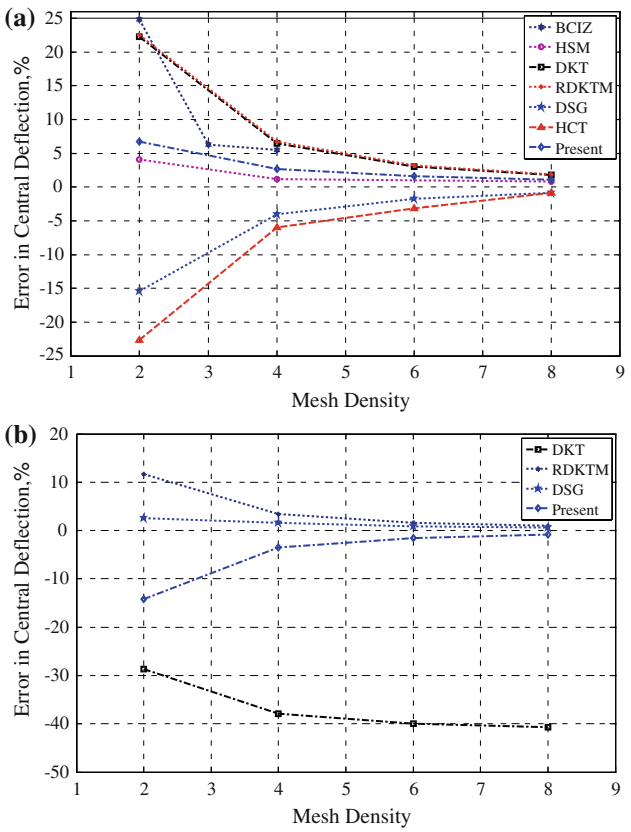

Fig. 8 Deflection at centre for a clamped square plate with uniform load for different element types. **a** Thin plate ($L/t = 100$). **b** Thick plate ($L/t = 5$)

which include HCT [34], HSM [35], BCIZ [36], DKT [37], RDKTM [14] and DSG [16], and the analytic solutions got from Ref. [31].

Numerical results of normalized central deflection for all cases are given in Tables 1, 2, 3, 4 and 5. The relative errors of the results are plotted in Figs. 7, 8, and 9, in which the label "mesh density" of the horizontal axes refers to the number of elements per side. From the results, it can be seen that the present method has a high accuracy and possesses fast convergence for both the thick and thin plates with different boundary conditions. For all studied cases, the proposed ES-FEM is not the best for each of the cases, but it is always among the bests for all these cases, which show clearly the stable and well-balanced feature of the ES-FEM. Note that the present method is very simple in formulation and no extra sampling points are introduced, compared with other elements.

3.3 Shear locking test

A simply supported or clamped square plate subjected to a uniform loading is used to test the shear locking phenomenon. The geometry and material properties are as same as those used in the previous subsection. The deflection is normalized as $\hat{w} = w_c D/qL^4$ and a 6×6 mesh is used here, and the computed results are plotted in Fig. 10. The results show clearly that the proposed method can avoid shear locking successfully and it provides excellent results regardless of the thickness of the plate.

3.4 Circular plate

A simply supported or clamped circular plate subjected to uniform loading is analyzed to demonstrate more features of the present method. The radius of the plate is $R = 5$ and two cases of the thickness, $t = 0.1$ and $t = 1$, are investigated here. Poisson ratio ν of the material is taken to be 0.3; Young's modulus E of the material is 3×10^5. The configuration and mesh information of the plate are shown in Fig. 11, where a quarter of the plate is modeled because of the symmetry conditions. A set of three meshes, 6, 24 and 96 elements, are employed here. The boundary conditions are given by:

$$\begin{aligned} &\text{Simply supported: } w = 0 \quad \text{on the boundary} \\ &\text{Clamped: } u = v = w = \theta_x = \theta_y = 0 \quad \text{on the boundary} \end{aligned} \tag{47}$$

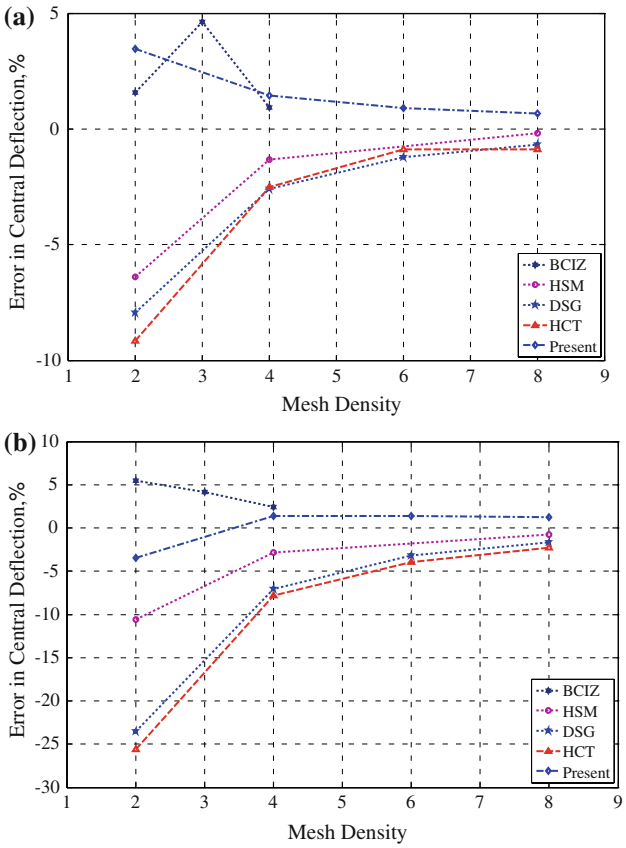

Fig. 9 Deflection at centre for a thin square plate ($L/t = 100$) with concentrated central load for different element types subjected different boundary. **a** Simply supported square plate. **b** Clamped square plate

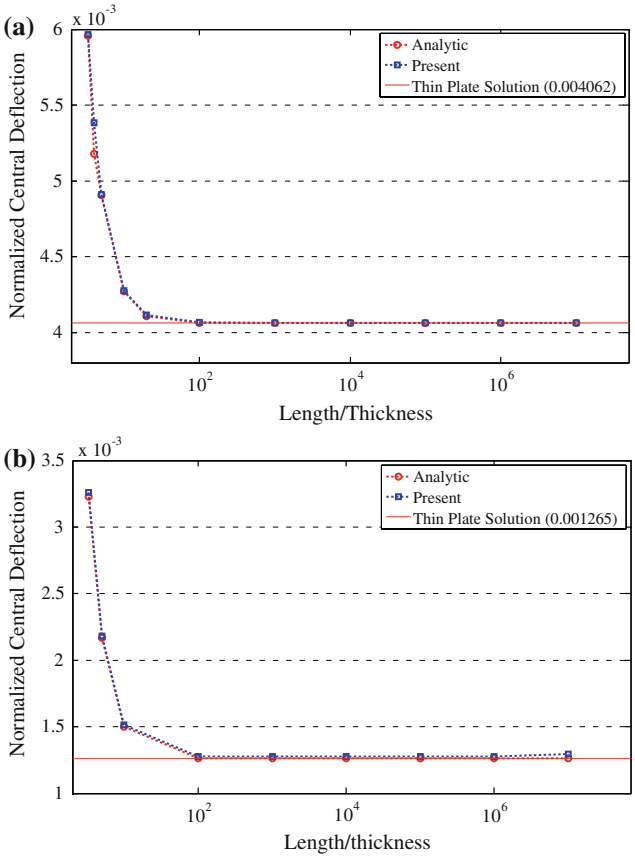

Fig. 10 Shear locking test. **a** simply supported square plate. **b** Clamped square plate

Fig. 11 Circular plate with uniform load. Geometry and Mesh arrangements

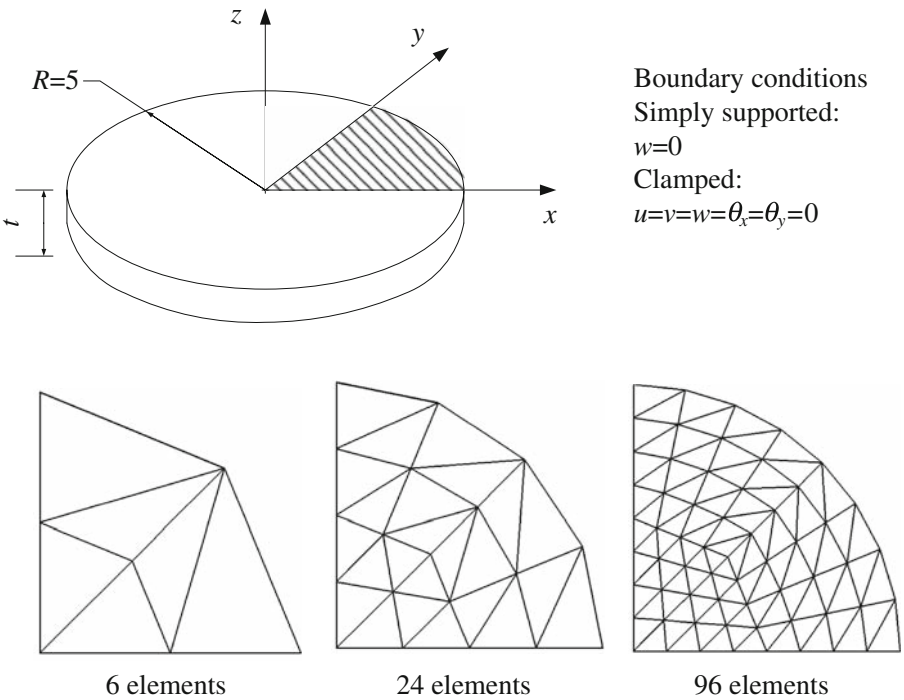

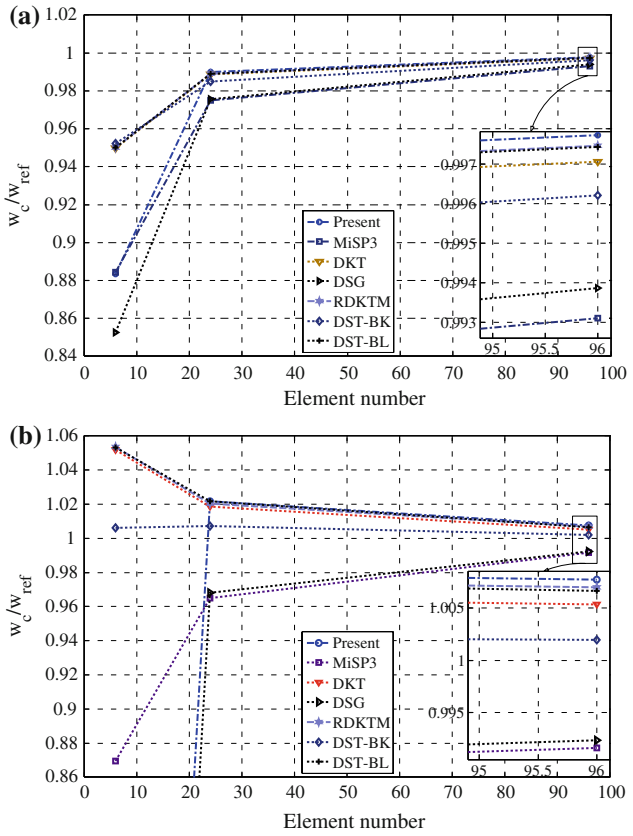

Fig. 12 Deflection at centre for a thin circular plate ($t/R = 0.02$) with uniform load for different element types. **a** Simply supported plate. **b** Clamped plate

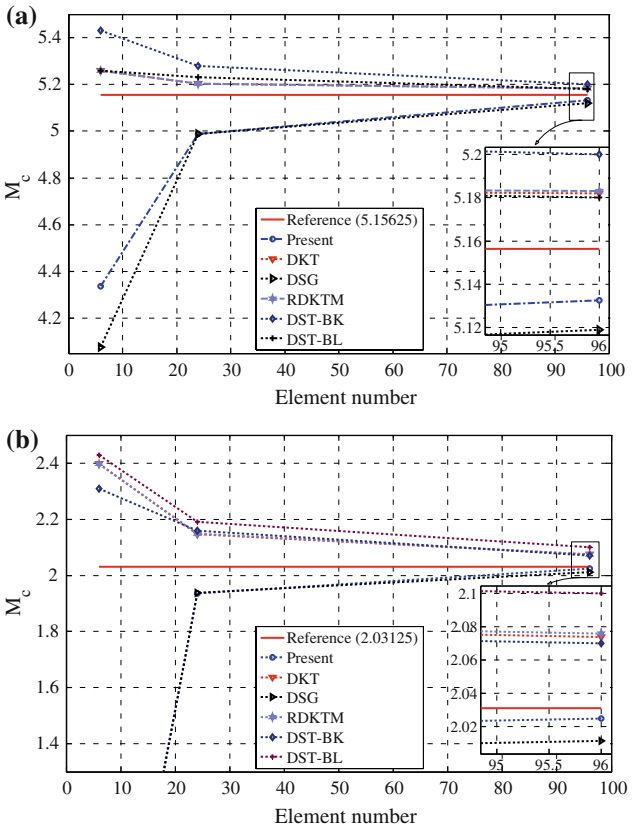

Fig. 13 Moment at centre for a thin circular plate ($t/R = 0.02$) with uniform load for different element types. **a** Simply supported plate. **b** Clamped plate

For a simply supported or clamped thin circular plate subjected to uniform load q_0; the analytic solutions for central deflections w and moment M_r are given by [37]

$$\text{Simply supported:}\quad \begin{aligned} w &= \frac{q_0 R^4}{64D}\left(\frac{5+v}{1+v} + \frac{8}{3k(1-v)}\left(\frac{t}{R}\right)^2\right) \\ M_r &= \frac{q_0 R^2}{16}(3+v) \end{aligned} \tag{48}$$

$$\text{Clamped:}\quad \begin{aligned} w &= \frac{q_0 R^4}{64D}\left(1 + \frac{8}{3k(1-v)}\left(\frac{t}{R}\right)^2\right) \\ M_r &= \frac{q_0 R^2}{16}(1+v) \end{aligned} \tag{49}$$

where $D = Et^3/(12(1-v^2))$ is the bending stiffness.

Numerical results of the present method are compared with those of existing triangular elements, which include DKT [37], RDKTM [14], BST-BK [38], BST-BL [39], MiSP3 [10], and DSG [16]. Numerical results of normalized central deflection w_c/w_{ref}, in which w_{ref} is analytic results in Eqs. (48) and (49) for the thin plate ($t/R = 0.02$) are plotted against the elements number in Fig. 12. The results of central moment are plotted in Fig. 13. These two pictures show that the present method can produce very accurate results when the problem domain is descritized using a reasonably number of elements (24 and 96 elements for this case). When too few elements are used (6 elements for this case), results of the present method are found only better than the plain elements also using DSG to eliminate shear locking. This is because the ES-FEM relies on the sufficient number of edges for the smoothing operation to take effects. When the model has too few edges, it has no much difference compared to the plain elements. For the case of 6 elements, there are totally 12 edges and only half of them (6 interior edges) are being effectively smoothed. Therefore, we are not expecting an outstanding performance of the ES-FEM for this case. This founding agrees with those methods using smoothed Galerkin formulations [17]. With the increase of the number of elements (e.g., 24 and 96 elements), the ES-FEM clearly out performs other elements. Note that in any practical problems, we use a lot more than tens of elements, and hence ES-FEM is expected to perform well in solving actual problems.

A clamped thin ($t/R = 0.02$) and thick ($t/R = 0.2$) circular plates subjected to a uniform load are analyzed to obtain the distributed bending moments (M_r, M_θ) and shear force (T_r). The mesh of 96 elements is employed, and the numerical results of present method are shown in Figs. 14, 15 and 16, together with the results obtained using BST-BK [38], BST-BL [39] and MiSP3 [10] with the same mesh.

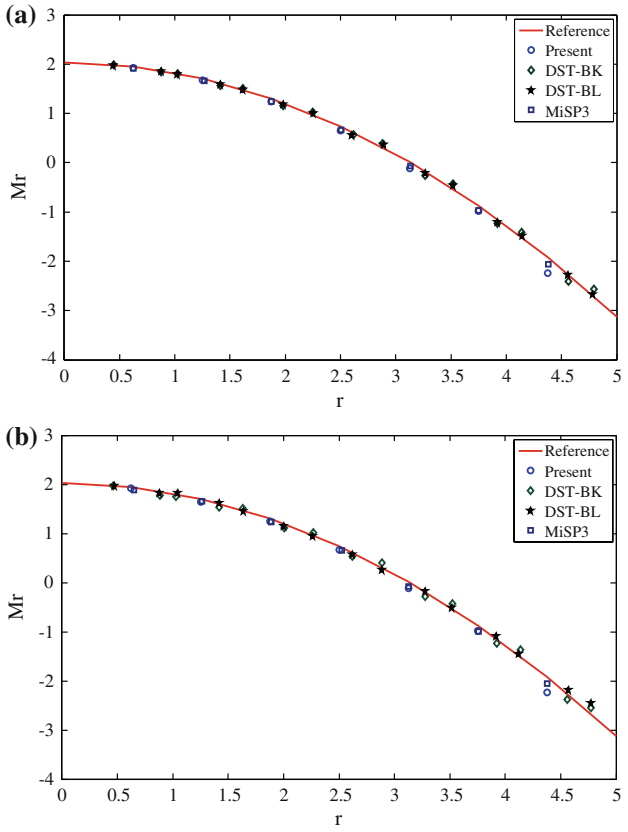

Fig. 14 Moment M_r along the radius for a clamped circular plate with uniform load. **a** Thin plate ($t/R = 0.02$). **b** Thick plate ($t/R = 0.2$)

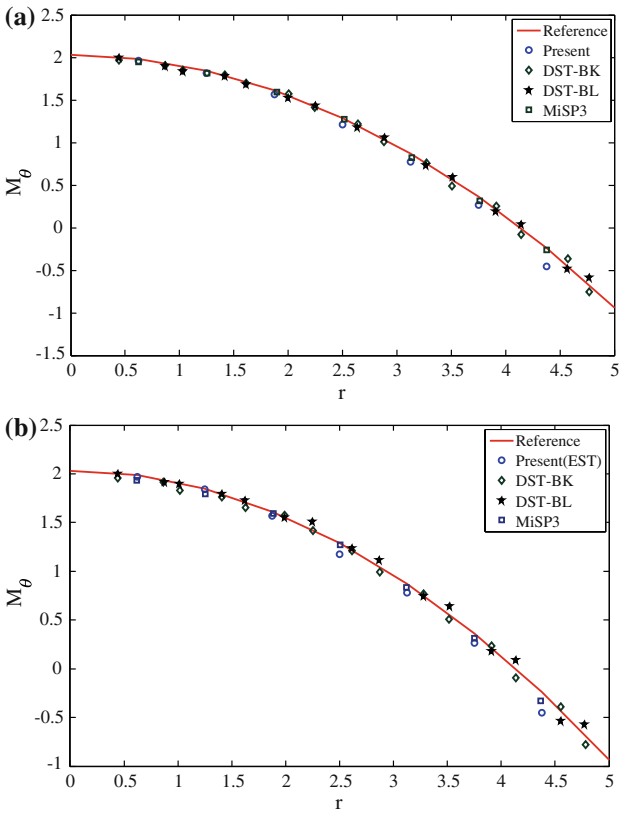

Fig. 15 Moment M_θ along the radius for a clamped circular plate with uniform load. **a** Thin plate ($t/R = 0.02$). **b** Thick plate ($t/R = 0.2$)

The analytic solutions are given by [40] as follows

$$\begin{aligned} M_r(r) &= \frac{q_0}{16}\left[(1+\upsilon)R^2 - (3+\upsilon)r^2\right] \\ M_\theta(r) &= \frac{q_0}{16}\left[(1+\upsilon)R^2 - (1+3\upsilon)r^2\right] \\ T_r(r) &= -\frac{q_0 r}{2} \end{aligned} \tag{50}$$

where r is the distance gauged from the plate center, and $D = Et^3/(12(1-\nu^2))$ is the bending stiffness.

Nodal values of M_r, M_θ and T_r for present method are obtained by averaging the values of the associated smoothing domains. The forces of the MiSP3 element are computed at the nodes, and the forces of BST-BL and BST-BK elements are computed at the centroids of the elements. It is found that the present method performs among the best for all the cases of both thin and thick plates. For bending moments, numerical results of all the methods studied here are all in good agreement with the reference solutions. For shear forces, the present method and MiSP3 element provide more accurate results compared with other numerical methods.

3.5 Pinched cylinder with end diaphragms

A pinched cylinder supported at each end by rigid diaphragm shown in Fig. 17 is considered in this section. It is a widely used benchmark problem for determining the ability of the elements to represent inextensional bending and complex membrane states. The length of the pinched cylinder is $L = 600$ in., the radius is $R = 300$ in., and the thickness is $t = 3$ in. The material properties are: Poisson's ratio $\upsilon = 0.3$, and Young's modulus $E = 3.0 \times 10^6$ N/in.^{2}. The loading is a pair of pinching loads $P = 100$ N. Owing to the symmetry, only 1/8 of the problem is modeled. Five meshes, 4×4, 6×6, 8×8, 12×12 and 16×16, are examined here and only the 4×4 mesh is shown in Fig. 17. In this case, the analytical solution of the radial displacement under the point load is 0.0018248 in., and the solutions given in this case are normalized with this value. Numerical results of the present method are compared with those of existing triangular shell elements ANS6S [11], C0 [41], DSG3 [16] and S3R element in ABAQUS©. From the results given in Table 6, it can be seen that the proposed element provides accurate results and has a good convergence performance.

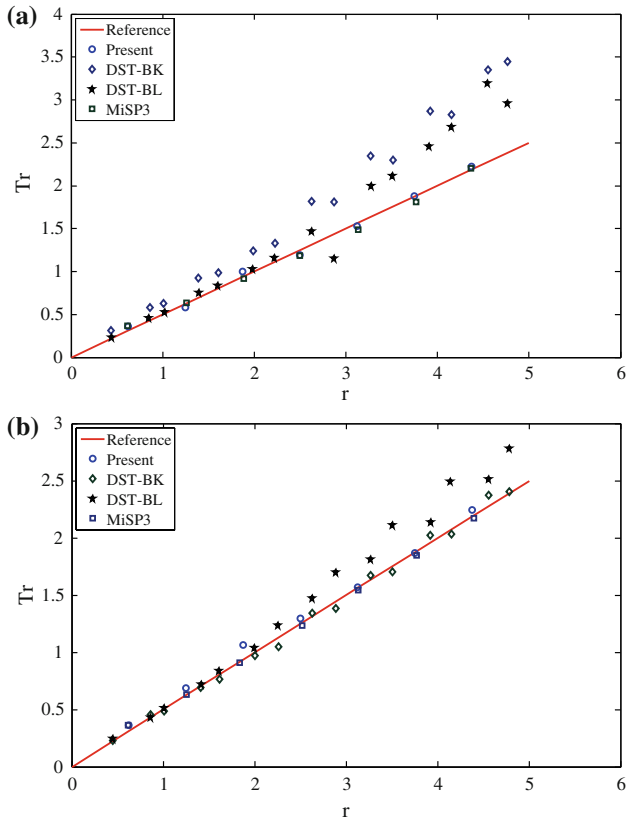

Fig. 16 Shear force T_r along the radius for a clamped circular plate with uniform load. **a** Thin plate ($t/R = 0.02$). **b** Thick plate ($t/R = 0.2$)

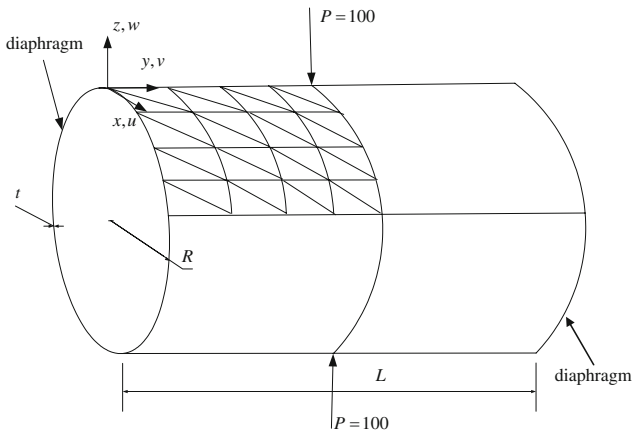

Fig. 17 Pinched cylinder with end diaphragms, 4 × 4 mesh illustrated

3.6 Hemispherical shell

The hemispherical shell with an 18∘ hole is loaded antisymmetrically by point loads as shown in Fig. 18. It exhibits almost no membrane strains but it is a challenging test on the ability of an element to handle rigid body rotations about normals to the shells surface. The geometric parameters are radius $R = 10$ m and thickness $t = 0.04$ m. The material

Table 6 Pinched cylinder with end diaphragms; normalized displacement at load point (the value used for normalization is 0.0018248 in)

Mesh	4 × 4	6 × 6	8 × 8	12 × 12	16 × 16
ANS6S	0.502	0.741	0.857	0.955	0.985
S3R	0.550	–	0.801	0.897	0.937
C0	0.300	0.530	0.670	–	–
DSG	0.313	0.548	0.690	0.832	0.897
Present	0.421	0.674	0.806	0.924	0.972

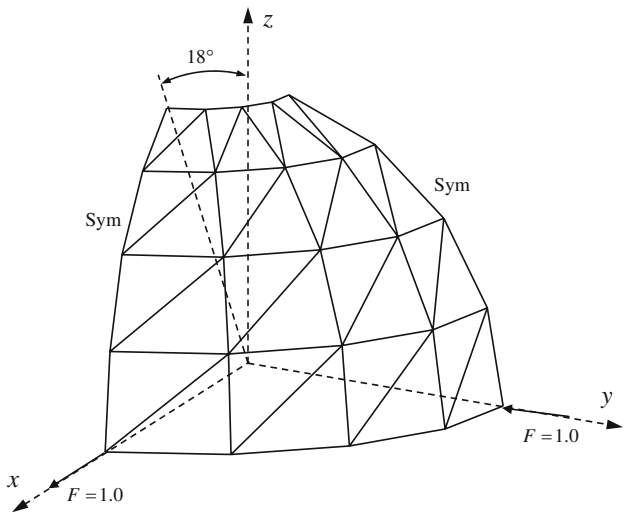

Fig. 18 Pinched cylindrical with end diaphragms, five nodes per side illustrated

Table 7 Hemispherical shell; normalized displacement at load point (the value used for normalization is 0.093 m)

Mesh	4 × 4	6 × 6	8 × 8	12 × 12	16 × 16
ANS6S	0.949	–	0.982	0.995	1.001
S3R	0.357	–	0.913	0.968	0.981
C0	0.870	0.930	0.960	–	–
DSG	0.965	0.977	0.981	0.986	0.989
Present	1.021	1.010	1.004	1.002	1.002

properties are: Poisson's ratio $\upsilon = 0.3$, and Young's modulus $E = 6.825 \times 10^7$ Pa. The point loading is $F = 1$ N. The solutions are obtained by using five meshes including $4 \times 4, 6 \times 6, 8 \times 8, 12 \times 12$ and 16×16. A typical 4×4 mesh is shown in Fig. 18. The analytical radial deflection coincident at point load is 0.093 m, and the solutions given in Table 7 are normalized with this value. It can be observed that the present results agree well with analytic solutions.

3.7 Hood of an automobile

Finally, an actual structure component of a car hood shown in Fig. 19 is studied using the present element. The dent resis-

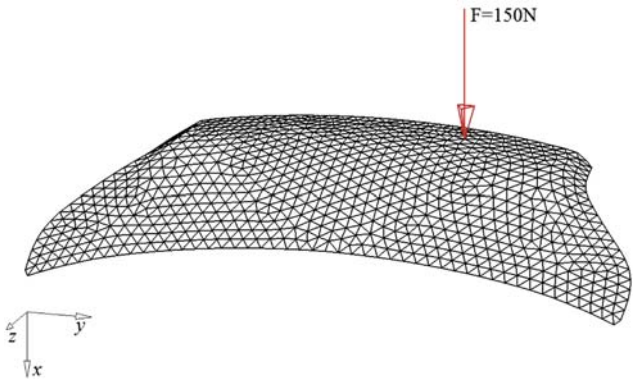

Fig. 19 Model of the hood of an automobile

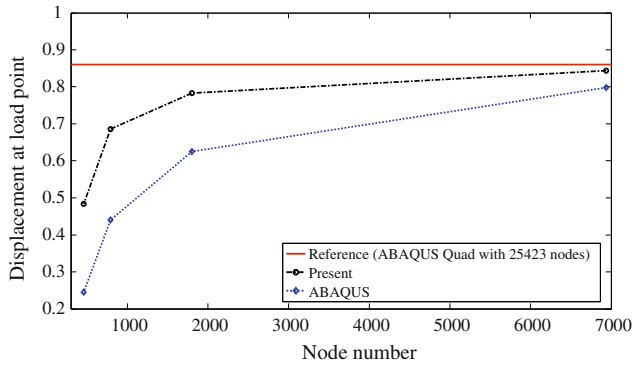

Fig. 20 Displacements in x-direction at the loading point

tance of car hood is one of the important considerations in the process of car design. In this example, all of the boundary nodes are fixed, and a concentrated load $F = 150$ N is imposed along the x-direction. The thickness of the thin shell is 0.8 mm; Poisson's ratio of the material is taken to be 0.3; Young's modulus of the material is 2.1×10^5 'N/mm^2. In order to test the accuracy of the present element, the solutions of triangular element S3R in ABAQUS© is used for comparison. The reference solution is obtained using quadrilateral shell elements in ABAQUS© with large number of (25,423) nodes. Figure 20 shows that the present triangular element has a much higher accuracy than triangular shell elements used in the ABAQUS©.

4 Conclusions

In this paper, an edge-based smoothed finite element method is formulated to analyze plates and shells using simple 3-node triangular elements. The smoothed Galerkin weak form is used for discretizing the system equations and the numerical integration is performed based on the smoothing domains associated with edges of the mesh. The Discrete Shear Gap method (DSG) is employed to mitigate the shear locking effect. Numerical results of plate and shell problems have confirmed the following features of the present method.

1. The conventional 3-node triangular element is used in the ES-FEM. There is no extra sampling point introduced to evaluate the stiffness matrix in present formulation. Hence the present method is very simple and can be easily implemented with little changes to the FEM code.
2. Compared with fully compatible displacement-based and hence overly stiff finite element, the present method can provide a much needed softening effect to the model owing to the edge-based gradient smoothing operation. Therefore, the performance of the present method is greatly enhanced.
3. The present method can pass exactly the pure bending patch test which ensures numerically the convergence of the proposed method.
4. Numerical comparisons show that the present element can obtain very stable and accurate results.

Acknowledgments The support of National 973 project (2010CB-328005), National Outstanding Youth Foundation (50625519), Key Project of National Science Foundation of China (60635020), Program for Changjiang Scholar and Innovative Research Team in University and the China-funded Postgraduates' Studying Abroad Program for Building Top University are gratefully acknowledged. The authors also give sincerely thanks to the partition financial support by the A*Star Singapore and the Centre for ACES, Singapore-MIT Alliance (SMA), and National University of Singapore.

References

1. Pugh ED, Hinton E, Zienkiewicz OC (1978) A study of triangular plate bending element with reduced integration. Int J Numer Methods Eng 12:1059–1078
2. Belytschko T, Stolarski H, Carpenter N (1984) A C0 triangular plate element with one-point quadrature. Int J Numer Methods Eng 20:787–802
3. Stricklin J, Haisler W, Tisdale P, Gunderson R (1969) A rapidly converging triangular plate bending element. AIAA J 7:180–181
4. Dhatt G (1969) Numerical analysis of thin shells by curved triangular elements based on discrete Kirchhoff hypothesis. In: Proceedings of the ASCE symposium on applications of FEM in civil engineering. Vanderbilt University, Nashville, pp 255–278
5. Dhatt G (1970) An efficient triangular shell element (Kirchhoff triangular shell element design via linear shell theory). AIAA J. 8:2100–2102
6. Batoz JL, Bathe KJ, Ho LW (1980) A study of three-node triangular plate bending elements. Int J Numer Methods Eng 15:1771–1812
7. Bathe KJ, Brezzi F (1989) The MITC7 and MITC9 plate bending element. Comput Struct 32:797–814
8. Lee PS, Bathe KJ (2004) Development of MITC isotropic triangular shell finite elements. Comput Struct 82:945–962
9. Lee PS, Noh HC, Bathe KJ (2007) Insight into 3-node triangular shell finite element: the effects of element isotropy and mesh patterns. Comput Struct 85:404–418

10. Ayad R, Dhatt G, Batoz JL (1998) A new hybrid-mixed variational approach for Reissner–Mindlin plates, the MiSP model. Int J Numer Methods Eng 42:1149–1479
11. Sze KY, Zhu D (1999) A quadratic assumed natural strain shell curved triangular element. Comp Methods Appl Mech Eng 174: 57–71
12. Kim JH, Kim YH (2002) Three-node macro triangular shell element based on the assumed natural strains. Comput Mech 29:441–458
13. Kim JH, Kim YH (2002) A three-node C0 ANS element for geometrically non-linear structural analysis. Comp Methods Appl Mech Engrg 191:4035–4059
14. Chen WJ, Cheung YK (2001) Refined 9-Dof triangular Mindin plate elements. Int J Numer Methods Eng 51:1259–1281
15. Chen WJ (2004) Refined 15-DOF triangular discrete degenerated shell element. Int J Numer Methods Eng 60:1817–1846
16. Bletzinger KU, Bischoff M, Ramm E (2000) A unified approach for shear-locking-free triangular and rectangular shell finite elements. Comput Struct 75:321–334
17. Liu GR (2008) A generalized gradient smoothing technique and smoothed bilinear form for Galerkin formulation of a wide class of computational methods. Int J Comput Methods 5(2):199–236
18. Liu GR (2009) A G space theory and weakened weak (W2) form for a unified formulation of compatible and incompatible methods, Part I: theory and part II: applications to solid mechanics problems. Int J Numer Methods Eng. doi:10.1002/nme.2719 (published online)
19. Chen JS, Wu CT, Yoon S, You Y (2001) A stabilized conforming nodal integration for Galerkin meshfree methods. Int J Numer Methods Eng 50:435–466
20. Liu GR, Zhang GY, Dai KY, Wang YY, Zhong ZH, Li GY, Han X (2005) A linearly conforming point interpolation method (LC-PIM) for 2D solid mechanics problems. Int J Comput Methods 2:645–665
21. Liu GR, Zhang GY (2008) Upper bound solution to elasticity problems: A unique property of the linearly conforming point interpolation method (LC-PIM). Int J Numer Methods Eng 74:1128–1161
22. Liu GR, Dai KY, Nguyen TT (2007) A smoothed finite element method for mechanics problems. Comput Mech 39:859–877
23. Dai KY, Liu GR, Nguyen TT (2007) An n-sided polygonal smoothed finite element method (nSFEM) for solid mechanics. Finite Elem Anal Des 43:847–860
24. Liu GR, Nguyen TT, Dai KY, Lam KY (2007) Theoretical aspects of the smoothed finite element method (SFEM). Int J Numer Methods Eng 71:902–930
25. Cui XY, Liu GR, Li GY, Zhao X, Nguyen TT, Sun GY (2008) A smoothed finite element method (SFEM) for linear and geometrically nonlinear analysis of plates and shells. CMES Comput Model Eng Sci 28(2):109–126
26. Nguyen-Xuan H, Rabczuk T, Bordas S, Debongnie JF (2008) A smoothed finite element method for plate analysis. Comp Methods Appl Mech Eng 197:1184–1203
27. Bathe KJ, Dvorkin EH (1985) A four-node plate bending element based on Mindlin–Reissner plate theory and mixed interpolation. Int J Numer Methods Eng 21:367–383
28. Liu GR (2009) On the G space theory. Int J Comput Methods 6(2):257–289
29. Liu GR, Nguyen TT, Dai KY, Lam KY (2008) An edge-based smoothed finite element method (ES-FEM) for static, free and forced vibration analysis. J Sound Vib 320:1100–1130
30. Cui XY, Liu GR, Li GY, Zhang GY, Sun GY (2009) Analysis of elastic–plastic problems using edge-based smoothed finite element. Int J Press Vessel Pip 86:711–718
31. Timoshenko S, Woinowsky-Krieger S (1940) Theory of plates and shells. McGraw-Hill, New York
32. Liu GR, Quek SS (2003) The finite element method: a practical course. Butterworth Heinemann, Oxford
33. Zienkiewicz OC, Taylor RL (2000) The finite element method. In: Solid Mechanics, 5th edn, vol. 2. Butterworth-Heinemann, Oxford
34. Clough RW, Tocher JL (1965) Finite element stiffness matrices for analysis of plates in bending. In: Proceedings of conference on matrix methods in structural mechanics. Air Force Institute of Technology, Wright-Patterson A. F. Base, Ohio, pp 515–545
35. Alwood RJ, Cornes GM (1969) A polygonal finite element for plate bending problems using the assumed stress approach. Int J Numer Methods Eng 1:135–149
36. Bazeley GP, Cheung YK, Irons BM, Zienkiewicz OC (1965) Triangular elements in plate bending conforming and non-conforming solutions. In: Proceedings of conference on matrix methods in structural mechanics. Air Force Institute of Technology, Wright-Patterson A. F. Base, Ohio, pp 547–577
37. Batoz JL (1982) An explicit formulation for an efficient triangular plate-bending element. Int J Numer Methods Eng 18:1077–1089
38. Batoz JL, Katili I (1992) On a simple triangular Reissner/Mindlin plate element based on incompatible modes and discrete constraints. Int J Numer Methods Eng 35:1603–1632
39. Batoz JL, Lardeur P (1989) A discrete shear triangular nine dof element for the analysis of thick to very thin plates. Int J Numer Methods Eng 28:533–560
40. Ugural AC (1981) Stresses in plates and shells. McGraw-Hill, New York
41. Belytschko T, Stolarski H, Carpenter NA (1984) C0 triangular plate element with one point quadrature. Int J Numer Methods Eng 20:787–862